HHS Public Access

Author manuscript

Photochem Photobiol. Author manuscript; available in PMC 2021 July 08.

Published in final edited form as:

Photochem Photobiol. 2021 January ; 97(1): 180–191. doi:10.1111/php.13321.

The endogenous tryptophan-derived photoproduct 6-formylindolo[3,2-b]carbazole (FICZ) is a nanomolar photosensitizer that can be harnessed for the photodynamic elimination of skin cancer cells *in vitro* and *in vivo*

Rebecca Justiniano[1], **Lohanna de Faria Lopes**[2], **Jessica Perer**[1], **Anh Hua**[1], **Sophia L. Park**[1], **Jana Jandova**[1], **Maurício S. Baptista**[2], **Georg T. Wondrak**[1,*]

[1]Department of Pharmacology and Toxicology, College of Pharmacy and UA Cancer Center, University of Arizona, Tucson, Arizona, USA

[2]Biochemistry Department, Institute of Chemistry, University of São Paulo, São Paulo, Brazil

Abstract

UV-chromophores contained in human skin may act as endogenous sensitizers of photooxidative stress and can be employed therapeutically for the photodynamic elimination of malignant cells. Here we report that 6-formylindolo[3,2-b]carbazole (FICZ), a tryptophan-derived photoproduct and endogenous aryl hydrocarbon receptor agonist, displays activity as a nanomolar sensitizer of photooxidative stress, causing the photodynamic elimination of human melanoma and nonmelanoma skin cancer cells *in vitro* and *in vivo*. FICZ is an efficient UVA/Visible photosensitizer having absorbance maximum at 390 nm (ε = 9180 $Lmol^{-1}cm^{-1}$), and fluorescence and singlet oxygen quantum yields of 0.15 and 0.5, respectively, in methanol. In a panel of cultured human squamous cell carcinoma and melanoma skin cancer cells (SCC-25, HaCaT-ras II-4, A375, G361, LOX), photodynamic induction of cell death was elicited by the combined action of solar simulated UVA (6.6 J/cm^2) and FICZ (≥ 10 nM), preceded by the induction of oxidative stress as substantiated by MitoSOX Red fluorescence microscopy, comet detection of Fpg-sensitive oxidative genomic lesions, and upregulated stress response gene expression (*HMOX1*, *HSPA1A*, *HSPA6*). In SKH1 'high-risk' mouse skin, an experimental FICZ/UVA photodynamic treatment regimen blocked the progression of UV-induced tumorigenesis suggesting feasibility of harnessing FICZ for the photooxidative elimination of malignant cells *in vivo*.

INTRODUCTION

Solar photoexcitation of specific endogenous skin chromophores acting as photosensitizers (including protoporphyrin IX, riboflavin, pyridoxal, pterin, urocanic acid, lipofuscin, advanced glycation endproducts, etc.) is thought to contribute to photooxidative stress involved in skin photocarcinogenesis and photoaging (1–10). Remarkably, endogenous skin

*Corresponding author wondrak@pharmacy.arizona.edu (Georg T. Wondrak).

Conflicts of Interest: The authors declare no conflict of interest.

chromophores may not only act as pathologically-relevant sensitizers of photooxidative stress but can also serve as therapeutic agents for the photodynamic elimination of malignant cells, a molecular strategy referred to as ‘photodynamic therapy’ (PDT) (5, 11–19). PDT involves the therapeutic induction of cell death downstream of photoexcitation of a sensitizer drug that generates cytotoxic reactive oxygen species (ROS) including singlet oxygen, downstream of photosensitizer-dependent electron and energy transfer mechanisms activating molecular ground-state oxygen (20). PDT-induced photooxidative stress can be harnessed for diverse dermatological applications targeting pathologies including microbial infection, acne, psoriasis, precancerous lesions (actinic keratosis), and various malignancies including BCC, SCC, and potentially melanoma (16, 18, 19, 21, 22).

Shortly after Raab’s, Jodlbauer’s, Jesionek’s and von Tappeiner’s seminal observations of the oxygen-dependent lethal effects of sunlight and fluorescent dyes on protozoa and skin carcinoma cells that was referred to as ‘photodynamic’, Meyer-Betz in 1913 noticed prolonged severe phototoxicity upon self-injection of sulfuric acid-extracted human blood and thereby established the potential photodynamic action of chromophores derived from human tissue, i.e. hematoporphyrin, on human skin (19, 23, 24). The potential utility of endogenous photosensitizers as therapeutic agents for the clinically-relevant elimination of cancer cells became apparent by the demonstration that co-exposure of hematoporphyrin-derivative (HpD) and light caused mammary tumor eradication in mice, followed by a seminal clinical trial (examining HpD-based PDT for locally recurrent breast carcinoma following mastectomy) and FDA approval in 1995 (11, 12). Strikingly, in addition to endogenous porphyrin-derivatives other cutaneous photosensitizers such as riboflavin (vitamin B_2) have attracted considerable attention serving as potential investigational drugs for PDT (1, 15, 25, 26).

Recently, we have reported that 6-formylindolo[3,2-b]carbazole (FICZ; Fig. 1a), an established tryptophan photoproduct and endogenous high affinity aryl hydrocarbon receptor (AhR) agonist that impacts skin barrier function, displays activity as an endogenous ultrapotent photosensitizer (27–30). Our experiments performed in human HaCaT, primary epidermal keratinocytes, and skin reconstructs exposed to UVA- and visible light photons demonstrated that UVA and blue light photoexcitation of FICZ induces photooxidative cellular stress (28, 31, 32). It is well established that tryptophan photolysis generates photoproducts with AhR-directed ligand activity leading to upregulation of cytochrome P450 gene expression (including *CYP1A1*) in skin cells. Specific tryptophan photoproducts [sharing an indolocarbazole-core including FICZ, indolo[3,2-b]carbazole (ICZ), 6,12-di-formylindolo[3,2-b]carbazole (dFICZ), and the FICZ oxidation product indolo[3,2-b]carbazole-6-carboxylic acid (CICZ)] are potent AhR agonists (27, 33–37). Among these tryptophan-derived photoproducts, FICZ displays extraordinary activity as an AhR ligand with almost ten times higher AhR binding affinity than 2,3,7,8-tetrachlorodibenzodioxin (TCDD), and FICZ-induced AhR activation is thought to contribute to photobiological effects in skin exposed to solar radiation (27, 30, 35, 37). In addition to its origin from photochemical pathways that dictate FICZ formation in skin cells, FICZ has also been identified as a microbiome-derived metabolite observable in clinical seborrheic dermatitis and pityriasis versicolor skin specimens (38). Moreover, inhibition of *CYP1A1*-dependent clearance of FICZ has been substantiated as a physiological mechanism underlying AhR

activation and FICZ potentiation (32, 39). However, specific quantitative yield of photochemical formation of FICZ from tryptophan and its photochemical and metabolic transformation products detectable *in vivo* remain a subject of ongoing research activities (35–37, 40, 41).

In addition to pronounced photosensitizer activity, this unique indolocarbazole-based chromophore displays a number of other unique molecular features not shared with other endogenous photosensitizers (37). Specifically, a rapid cellular turnover of FICZ occurs as a result of FICZ-driven AhR-dependent induction of *CYP1A1*, representing a negative feedback loop minimizing skin residence time of this photosensitizer (28, 39). It has also been demonstrated that potent and transient AhR activation by FICZ may cause other cutaneous effects including the attenuation of inflammation and autoimmunity as well as an enhancement of skin barrier function, activities now being an area of preclinical developmental efforts (29, 30, 37, 42, 43).

Given the common developmental origin of clinically relevant photosensitizers (first recognized as endogenous biochemical chromophores displaying phototoxic and then phototherapeutic effects in skin), we aimed at repurposing the endogenous photosensitizer FICZ as a novel experimental photodynamic agent for potential therapeutic gain. Here we report our prototype experiments that substantiate feasibility of FICZ-based PDT targeting cultured human malignant skin cells, epidermal reconstructs, and UV-induced tumorigenesis assessed in ‘high-risk’ SKH-1 mouse skin (44).

MATERIALS AND METHODS

Chemicals:

FICZ (CAS#:172922-91-7) was purchased from Enzo (Plymouth Meeting, PA) and prepared in DMSO as a 1mM stock. Other chemical reagents were from Sigma (St Louis, MO).

Photophysics:

Determinations were performed following procedures as described earlier (45, 46). Absorption spectra were registered in a Shimadzu spectrophotometer (UV-2400-PC) and the molar extinction coefficient (ε) was determined in methanol by plotting the absorption at the wavelength of maximum absorbance (λ_{max} = 390 nm) as a function of photosensitizer concentration and by applying Beer-Lambert law. Fluorescence spectra were recorded in a Varian Cary Eclipse spectrofluorometer. The fluorescence quantum yield (Φ_f) was obtained in methanol by measuring and comparing the area under the emission spectrum of FICZ with that of a known standard, i.e., quinine sulfate (QS) in 0.5 mol·L^{-1} of sulfuric acid solution (Φ_f=0.55). Corrections for differences in refractive index followed classical procedure (equation 1, Fig. 1). Absorbance values of standard and sample were both of 0.07 at the excitation wavelength (390 nm). The quantum yield of singlet oxygen generation (Φ_Δ) was determined by using a NIR fluorometer (Edinburg Instruments) equipped with a liquid-nitrogen cooled Hamamatsu PMT (R55009) and using a CryLaS 355/532 nm laser as excitation source. Singlet oxygen emission spectra was obtained by scanning emission monochromator from 1200 to 1350 nm and by acquiring emission intensity every 3 nm. The

$^1O_2$ quantum yields (Φ_Δ) was calculated by comparing the integrated area under the spectra of FICZ with that of a known standard (phenalenone, Φ_Δ=0.97). Both sample and standard were dissolved in methanol to provide absorbance of 0.2 at 355 nm; calculations were done (equation 2, Fig. 1).

Cell culture:

Human malignant melanoma cells A375, LOX (ATCC) were cultures in RPMI and human malignant melanoma cells G-361 (ATCC) were cultured in McCoy's 5a medium. The human squamous cell carcinoma cell line SCC-25 (ATCC) were cultured in Dulbecco's Modified Eagle Medium/Nutrient Mixture F-12 Hams (DMEM-F12). The locally invasive malignant human HaCaT-ras transformed II-4 keratinocyte line (representing c-Harvey-ras-oncogene transfected HaCaT cells) was provided by G. Tim Bowden (University of Arizona) and cultured in DMEM (44, 47). All media were supplemented with 10 % bovine calf serum (BCS). Cells were maintained at 37°C in 5% CO2, 95% air in a humidified incubator.

Irradiation:

Cells were irradiated with solar simulated UVA and blue light (LED 460 nm) as published earlier (9, 28, 48). Irradiation of cells, tissue samples, and mouse skin with solar simulated UVA was conducted utilizing a kilowatt large area light source solar simulator (model 91293, Oriel Corporation) equipped with a 1000W Xenon arc lamp and power supply, model 68920, and a VIS-IR bandpass blocking filter combined with an atmospheric attenuation filter (output 290–400 nm plus residual 650–800 nm). The output was quantified using a dosimeter from International Light Inc., model IL1700, with an SED240 detector for UVB (range 265–315 nm, peak 285 nm), or a SED033 detector for UVA (range 315–400 nm, peak 365 nm). Using UVB/C blocking filter, the dose at 365 mm from the source was 5.39 mJ/cm^2 sec UVA radiation with a residual UVB dose of 3.16 μJ/cm^2 sec. For blue light exposure, a commercial 15W LED (460 nm peak emission, 10 nm maximum oscillation; Sunshine Systems, Wheeling, IL) was used delivering visible light at an irradiance of 2.12 mW/cm^2 (450–470 nm) as determined using a spectroradiometer, model 754, from Optronic Laboratories (Orlando, FL). Cell exposure to UVA [(100,000 cells per 35 mm cell culture dish in PBS (1 ml with or without test compound)] occurred without lid; cells receiving visible radiation (at a distance of 50 mm from the source) were irradiated through the polystyrene lids (under 1 ml PBS).

Transmission electron microscopy:

Samples for transmission electron microscopy (TEM) were fixed in situ 2.5% glutaraldehyde in 0.1 M PIPES solution (pH 7.4), prepared and processed as described earlier (49). Specimens were examined using a Tecnai G2 Spirit transmission electron microscope (FEI, Hillsboro, OR) operated at 100 kV. Digital images were captured with a XR41 4-megpixel digital camera system (AMT, Danvers, MA).

Flow cytometric analysis of cell viability:

AnnexinV-FITC/propidium iodide assay was used to confirm the induction of cell death using an apoptosis detection kit following the manufacturer's protocol (APO-AF, Sigma, St. Louis, MO) as published previously (50).

Detection of intracellular oxidative stress:

Flow cytometric analysis of 2',7'-dichlorodihydrofluorescein diacetate (DCF-DA) as a non-fluorescent precursor dye was employed to measure intracellular ROS generation following our published standard procedure (28, 49).

Detection of mitochondrial superoxide:

A mitochondrial superoxide indicator MitoSOX™ Red (Invitrogen) was used to measure intramitochondrial superoxide production using fluorescent microscopy following the manufacturer's protocol (51). After PDT, cells were loaded with 5 μM MitoSOX and the nuclear counterstain Hoechst 33342 (Thermo-Fisher) in fresh medium for 10 mins at 37 °C and 5% CO_2 in the dark. Cells were then rinsed several times with DPBS and visualized by EVOS FL auto fluorescent microscope using the DAPI cube and RFP light cube. MitoSOX fluorescence of digital images was quantified using the imaging software Image J. (NIH; http://rsb.info.nih.gov/ij/download.html).

Assessment of lysosomal acidification:

To detect alterations in lysosomal acidification, cells were stained with LysoSensor™ Green DND-189 (ThermoFisher Scientific) and imaged with fluorescent microscopy following the manufacturer's protocol. In brief, after PDT at indicated time points, cells were incubated with 5 μM LysoSensor ™ and Hoechst® 33342 in fresh medium for 10 min at 37 °C and 5% CO_2 in the dark. Cells were then washed with DPBS and visualized under DPBS by EVOS FL auto fluorescent microscope using the DAPI and GFP light cube. The LysoSensor ™ fluorescence was quantified using Image J (49).

Assessment of mitochondrial transmembrane potential ($\Delta\psi m$):

The potentiometric dye 5,5',6,6'-tetrachloro-1,1',3,3'-tetraethylbenzimidazolyl-carbocyanine iodide (JC-1; Sigma, T4069) was used to examine the mitochondrial transmembrane potential [$\Delta\psi m$; JC-1 monomeric green fluorescence (depolarized mitochondria, detector FL-1) vs. JC-1 aggregate red fluorescence (polarized mitochondria, detector FL-2) fluorescence] following our published procedure (50).

Real time qPCR:

Total cellular RNA (3×10^6 cells) was isolated from cells using the RNeasy kit (Qiagen Valencia, CA, USA) following the manufacturer's instructions. Reverse transcription of RNA (200 ng of total RNA in a 50 μl reaction) was performed using the TaqMan Reverse Transcription Reagents (Roche Molecular Systems NJ, USA) following previously published procedures (50). Reverse transcription was primed with random hexamers and incubated at 25 ºC for 10 min followed by 48 ºC for 30 min, 95 ºC for 5 min, and cooled at 4 ºC. PCR reactions contained 3.75 μL of cDNA, 12.5 μL TaqMan Universal PCR Master Mix

(Roche Molecular Systems), 1.25 μL of the following gene specific primers: human *HSPA6* (Hs00275682_s1), *HSPA1A* (Hs00359163_s1), *HMOX1* (Hs00157965_m1and *ACTB* (Hs99999903_m1; (Applied Biosystems, Branchburg, NJ). Gene-expression levels were normalized to *ACTB* (β-actin). The comparative threshold cycle method (ΔΔCt) was used for quantification analysis following the ABI Prism 7000 sequence detection system user manual as described previously (28, 50).

Immunoblot analysis:

Immunoblot analysis was conducted following our published standard procedures (28). The following primary antibodies were used: Total p38 (#9212, Cell Signaling, Danvers, MA), phospho-p38 (#9211, Cell Signaling), total eIF2α (#9722, Cell Signaling), phospho-eIF2α (#9721, Cell Signaling), heme oxygenase I (#5853, Cell Signaling), HSP70/HSP72 monoclonal antibody (C92F3A-5, Enzo Life Sciences). Equal protein loading was assessed using immunostaining for ACTB (A4700, Sigma). The horseradish peroxidase-conjugated goat anti-rabbit (111–035-144) or goat anti-mouse secondary antibody (115–035-146, Jackson Immunological Research, West Grove, PA) was followed by visualization using enhanced chemiluminescence detection reagents (Thermofisher). For quantification of immunoblots, digital image analysis was performed using Image Studio™ Lite quantification software (LI-COR Biosciences, Lincoln, NE).

Comet assay (alkaline single-cell gel electrophoresis):

The alkaline comet assay was conducted following the manufacturer's protocol (Trevigen, Gaithersburg, MD) as described by us before (9, 28). Slides were stained with Hoechst, rinsed with DPBS and fluorescent comets were visualized by EVOS FL auto fluorescent microscope using the DAPI light cube. The average comet tail moments were calculated employing the Image J software. The average of 50 comets were calculated for each group and standardized to the untreated group (control). Oxidized purine bases were detected using the Fpg-FLARE assay according to the manufacturer's instructions (Trevigen).

Photodynamic treatment of human epidermal skin reconstructs:

EpiDerm tissues (EPI-200, 9 mm diameter, six-well format; MatTek, Ashland, MA) were treated with FICZ (100 nM final concentration in 0.9 ml EPI-200-ASY media per well), followed by culture at 37 ºC for 6 h. Before irradiation, inserts were rinsed with PBS and then exposed to UVA radiation (6.6 J/cm^2). After irradiation, tissue inserts were cultured for another 24 h in media. Tissue was then processed for paraffin embedment followed by hematoxylin and eosin staining, and immunohistochemical analysis detected cleaved caspase 3 employing a rabbit polyclonal primary antibody (Asp175) (Cell Signaling, Danvers, MA) as described previously (28).

Photodynamic treatment of SKH-1 mouse skin:

SKH-1 hairless female mice (Charles River Laboratories) were maintained under 12-h light/dark cycles receiving water and food *ad libitum*. At the beginning of the experiment, 8-week old mice (n=12) were divided into 4 groups (n=3): (1) control (DMSO only), (2) UVA + DMSO, (3) FICZ in DMSO, (4) UVA + FICZ in DMSO. Solar simulated UVA dose was 6.6

J/cm^2. 'FICZ' (in DMSO; 1 mM final concentration) or 'DMSO only' were applied topically to dorsal skin areas (20 μl total volume). After 10 min, UVA or mock irradiation were performed. Mice were maintained for another 48 h and then sacrificed. Dorsal skin was harvested and processed for (histo)-pathological examination and further IHC analysis (cleaved caspase 3; as described above). Animal experimental procedures and protocol have been reviewed and approved by the University of Arizona Institutional Animal Care and Use Committee (PHS Assurance No. A-3248-01; #11-316).

Photodynamic treatment of UV-exposed SKH1 high-risk (tumor-prone) hairless mouse skin:

A published standard procedure was followed (44). Six to eight-week old female SKH1 Elite™ hairless mice were purchased from Charles River Laboratories (Wilmington, MA) and housed and maintained in accordance with The University of Arizona Animal Care and Use Committee standards under an approved protocol. To generate the standard UV-exposed SKH-1 'high-risk' (tumor-prone) mouse model, SKH-1 mice were subjected to an 18-week UVB regimen [delivering 190 mJ/cm^2 per UV exposure (final dose); three times per week; first six weeks of UV exposure: increasing dose regimen (week 1–2: 40 %; week 3–4: 60 %; week 5–6: 80% of final dose per exposure) to allow skin photo-adaptation]. An irradiation panel of UVB-313 lamps (Q-LAB, Westlake, OH) was used. At the end of the 18 weeks irradiation period, these mice are tumor free but have a high risk for developing papilloma lesions over the next several weeks (44). These tumor free SKH1 'high risk' mice (4 per group) were then subjected to three cycles of experimental FICZ-PDT (FICZ: 1 mM in DMSO (20 μl); UVA: 6.6 J/cm^2 UVA, 3 PDT cycles) followed by quantitative determination of tumor multiplicity at the end of the experiment (week 22). For comparison, in parallel with the FICZ-PDT regimen, additional mice (4 per group) were exposed to 'UVA only', 'FICZ only', or 'mock' (DMSO only, no UVA) treatment. Animal experimental procedures and protocol have been reviewed and approved by the University of Arizona Institutional Animal Care and Use Committee (PHS Assurance No. A-3248-01; #11-316).

Statistics:

All results are presented as means: ± SD of at least three independent experiments ($n \geq 3$), unless indicated otherwise. Data were analyzed employing analysis of variance (ANOVA) with Tukey's post hoc test using the Prism 4.0 software; means without a common letter differ from each other ($p<0.05$). In the UV-induced skin tumorigenesis model, tumor multiplicity was compared between treatment groups employing Mann-Whitney nonparametric statistical analysis using the Prism 4.0 software ($p < 0.05$; 95% confidence interval).

RESULTS AND DISCUSSION

Assessment of photophysical properties of FICZ relevant to photodynamic effects

Following our previous studies demonstrating FICZ phototoxicity, a more detailed physicochemical characterization of FICZ was pursued (28). Specifically, building on previously published qualitative data, stringent quantification of key photophysical parameters including ε, Φ_f, and Φ_Δ was performed (Fig. 1). As observed before, the

absorption spectrum of FICZ exceeds the UV spectral range, covering the visible range up to 520 nm, displaying an appreciable extinction coefficient (ε = 9180 $mol \cdot L^{-1} \cdot cm^{-1}$) at 390 nm (Fig. 1a-b). FICZ is also able to fluoresce with wavelength maxima at 520 nm and Φ_f of 0.15 (methanol) (Fig. 1c-d). Although FICZ is a very efficient fluorophore in methanol, in aqueous solution it is highly aggregated barely displaying any fluorescence. However, it is likely that FICZ can disaggregate when bound to hydrophobic pockets of proteins (such as that of AhR, its major biological target). In order to test this hypothesis, we titrated FICZ aqueous solution with BSA (Fig. 1c; main graph). Indeed, FICZ fluorescence was restored in the presence of increasing concentrations of BSA, indicating that FICZ disaggregates upon binding to the BSA hydrophobic pocket. Strikingly, there are no previous reports indicating the generation of triplet states and $^1O_2$ by photo-excited FICZ, in spite of the fact that photoexcitation of this molecule has been implicated in a series of photoinduced ROS-mediated processes observable in cells and tissues (28). Thus, we initiated further investigations following our published standard procedures (45, 46). Strikingly, upon FICZ photoexcitation at 355 nm, the $^1O_2$ fingerprint emission band with maximum centered at 1,270 nm, which is due to the $O_2(a^1\Delta g) \rightarrow O_2(X^3\Sigma g-)$ transition, is observed (Fig. 1e). By comparing the NIR emission of FICZ with that of phenalenone (a known standard of singlet oxygen generation), we then calculated that Φ_Δ of FICZ is 0.53, indicating that FICZ is indeed a very efficient $^1O_2$ photosensitizer. $^1O_2$ is generated through energy transfer from a triplet excited state, indicating that FICZ also generates triplets, with yields at least as high as that of Φ_Δ. It is also worth mentioning that triplets can engage in type I reactions when present in close contact with a biological target.

FICZ/UVA-dependent photodynamic induction of cytotoxicity in cultured human skin cancer cells lines

Next, expanding on our prior studies demonstrating FICZ phototoxicity in cultured primary keratinocytes, feasibility of harnessing FICZ photodynamic activity for the light driven elimination of malignant cells was examined *in vitro* (28). To this end, a panel of cultured human malignant skin cell lines (A375 malignant melanoma, LOX metastatic melanoma, G361 metastatic melanoma; SCC-25 squamous cell carcinoma, HaCaT-ras II-4 malignant keratinocytes) was exposed to the isolated or combined action of FICZ (10–100 nM) and UVA (3.3 J/ cm^2), whereas control cells remained untreated (Fig. 2). Cell viability was then determined by flow cytometric analysis of annexinV (AV)-FITC/propidium iodide (PI)-stained cells, performed 24 h after photodynamic treatment (44). In all cell lines, a significant loss of viability was observed that occurred in response to the combined action of FICZ and UVA, an effect not achieved in response to the isolated exposure to either FICZ or UVA. SCC-25 carcinoma cells displayed the most pronounced sensitivity to photodynamic induction of cell death observable at FICZ concentrations as low as 10 nM (eliminating almost 75 % of live cells), whereas HaCaT-ras II-4 cells displayed a more resistant phenotype (with less than 20 % cells eliminated at 10 nM FICZ; Fig 2a-b).

FICZ/UVA-dependent induction of stress response gene expression and signaling in SCC-25 keratinocytes

Given the high sensitivity of SCC-25 to photodynamic elimination by FICZ/UVA treatment, we focused our pilot studies on these cells (Fig. 3–4), complemented by data obtained in

malignant melanoma cells (Fig. 5). First, since our previous research has demonstrated that FICZ displays pronounced absorptivity and fluorescence throughout the UVA and blue visible portions of the solar spectrum, we tested feasibility of photodynamic elimination of SCC-25 keratinocytes harnessing FICZ activation using a visible light source (LED; 460 nm) (Fig. 3a) (28). Remarkably, as observed with UVA photoexcitation, visible photoexcitation of FICZ (10 nM) displayed pronounced photodynamic activity (eliminating more than 60 % of live SCC-25 keratinocytes as assessed 24 h after treatment).

Next, the photodynamic mechanism of FICZ-dependent cytotoxicity targeting SCC-25 cells was explored in more detail complementing our previous mechanistic data obtained previously in primary human keratinocytes (Fig. 3b-f) (28). It was observed that FICZ photodynamic potency was attenuated if UVA exposure was performed in the presence of the singlet oxygen quencher NaN_3; in contrast, no cytoprotection was achieved when FICZ/UVA exposure occurred in the presence of the pan-caspase inhibitor z-VADfmk (Fig. 3b). Attempts to harness irradiation in deuterium oxide, used widely in photochemical experiments as another molecular probe indicative of singlet oxygen involvement, failed due to general cytotoxicity of the deuterium oxide-based PBS preparation (under which irradiation occurred), a confounding factor that interfered with data interpretation.

Taken together, these data are consistent with a mode of phototoxicity that involves formation of singlet oxygen upstream of caspase-independent execution of cell death, an observation reported by us earlier in primary human keratinocytes exposed to FICZ/UVA (28). Strikingly, cellular glutathione depletion [employing buthionine sulfoximine (BSO) pretreatment] caused further potentiation of FICZ photodynamic activity, an observation substantiating the involvement of photooxidative stress in FICZ/UVA cytotoxicity (Fig. 3d). Efficacy of BSO-induced depletion of reduced cellular glutathione in SCC-25 cells by more than 50% was substantiated using a luminescent assay (GSH-CellGlo™) [as employed by us before (data not shown)] (9).

To gain further mechanistic insights on molecular mechanisms underlying FICZ/UVA-induced cytotoxicity elicited in SCC-25 cells, stress response signaling and target gene expression were examined at the mRNA and proteins levels, employing real time RT-PCR and immunoblot analysis, respectively (Fig. 3c). Indeed, UVA/FICZ photodynamic treatment caused pronounced transcriptional upregulation of stress response target gene expression comprising (*i*) the oxidative stress response gene *HMOX1* (*heme oxygenase 1*; 3-fold), (*ii*) the heat shock response gene *HSPA6* [*heat shock protein family A (Hsp70) member 6*; 43-fold], and (*iii*) the xenobiotic response element (XRE)-controlled AhR target gene *CYP1A1* [*Cytochrome P450, family 1, subfamily A, polypeptide 1*; 20-fold) detectable within 6 h after exposure, an observation consistent with stress response gene expression as profiled and discussed by us in detail in human epidermal keratinocytes and mouse epidermis (28). As expected, only FICZ/UVA combination treatment efficiently upregulated *HMOX1* and *HSPA6* expression, whereas *CYP1A1* expression was elevated in response to FICZ treatment even in the absence of UVA exposure, an observation consistent with the AhR-directed ligand activity of FICZ (driving *CYP1A1* expression) that occurs independent of photon exposure as reported previously in HaCaT keratinocytes (28).

Immunoblot analysis then confirmed FICZ/UVA-induced gene expression changes at the protein level (Fig. 3e). Strikingly, within 1 h exposure time, FICZ/UVA treatment stimulated activational phosphorylation (Thr180/Tyr182) of the stress-activated MAPkinase p38 with concomitant inhibitory phosphorylation of eIF2α (eukaryotic translation initiation factor), established markers of skin cell exposure to oxidative and proteotoxic cellular stressors (3, 5, 9, 28, 29, 31). Furthermore, consistent with early induction of FICZ/UVA-imposed cell stress, pronounced upregulation of stress response protein expression (Hsp70, HO-1) was observed at 6 h after PDT (- a time point chosen to allow the stress-induced induction of expression at the protein level detectable by immunoblot analysis), a finding in accordance with changes detected at the mRNA level (*HSPA6*, *HMOX1*).

FICZ/UVA-dependent impairment of mitochondrial, lysosomal, and nuclear integrity in SCC-25 keratinocytes

Next, flow cytometric analysis using the potentiometric probe JC-1 revealed the photodynamic induction of mitochondrial transmembrane potential loss in response to UVA/FICZ combination treatment, an effect not observed in response to isolated FICZ or UVA exposure (Fig. 3f). To further substantiate the occurrence of mitochondrial disturbance in SCC-25 cells, we employed live cell fluorescence image analysis using the mitochondria-directed superoxide probe MitoSOX Red™ (Fig. 4a). Indeed, a pronounced almost 20-fold increase in MitoSOX Red™ fluorescence intensity (indicative of mitochondrial superoxide production) was detectable 60 min after FICZ/UVA photodynamic exposure. Mechanistically, it remains to be explored if increased superoxide formation as substantiated by fluorescence-imaging occurs as a result of FICZ-dependent singlet oxygen formation that might cause mitochondrial disturbance followed by increased superoxide leakage.

Next, following our earlier studies in cultured HaCaT and primary keratinocytes, photodynamic impairment of genomic integrity and induction of oxidative DNA damage was examined in malignant SCC-25 keratinocytes using alkaline single cell gel electrophoresis performed with or without formamidopyrimidine DNA-glycosylase (Fpg)-digestion (Fpg-modified comet assay) allowing the quantitative assessment of oxidative DNA damage (Fig. 4b) (9, 28). Indeed, FICZ/UVA exposure induced genotoxic stress in SCC-25 cells as evident from a pronounced increase in average comet tail moment (more than 6-fold over untreated control) observable within 1 h exposure time. Interestingly, without Fpg-digestion no comets were detectable in response to FICZ/UVA treatment, an observation suggesting that FICZ/UVA-induced impairment of genomic integrity depends on photodynamic induction of oxidative stress upstream of oxidative DNA base modification.

Since it has been shown earlier that lysosomal impairment is an important consequence of photodynamic exposure, we also examined the functional status of lysosomes in SCC-25 cells exposed to FICZ/UVA (Fig. 4c)(52, 53). Using the lysosomotropic pH indicator and functional probe Lysosensor Green™ in live cells, it was observed that photodynamic exposure caused rapid lysosomal dysfunction as evident from loss of lysosensor fluorescence, observed only in response to FICZ/UVA combination treatment (49).

Taken together, these data indicate that FICZ/UVA combination treatment of SCC-25 malignant keratinocytes is associated with rapid induction of superoxide generation and

transmembrane potential loss, nuclear oxidative DNA damage, and lysosomal dysfunction, all of which are well established occurrences compromising crucial organelle function as a hallmark of photodynamic cell damage.

FICZ/UVA-dependent induction of oxidative stress and impairment of mitochondrial, lysosomal, and nuclear genomic integrity in A375 malignant melanoma cells

After demonstrating photodynamic effects of FICZ/UVA exposure in SCC-25 malignant keratinocytes, we also assessed the cellular stress response elicited by this treatment in A375 malignant melanoma cells that displayed sensitivity to FICZ-dependent photodynamic elimination (Fig. 5). In analogy to cellular changes observed before in SCC-25 cells, transmission electron microscopy performed 6 h after FICZ-PDT (FICZ 100 nM; UVA 3.3 J/cm^2) revealed pronounced morphological changes including plasma membrane disintegration, cytosolic vacuolization, loss of functional organelles including mitochondria, and nuclear condensation (Fig. 5a). It was also observed that FICZ-dependent photodynamic elimination of A375 malignant melanoma cells can be achieved using a visible light source (LED; 460 nm) as established before with SCC-25 cells (Fig. 3a and 5b). Likewise, only FICZ/UVA combination treatment induced cellular oxidative stress as assessed by flow cytometric DCF-DA fluorescent staining of PDT-exposed cells (Fig. 5c). Since DCF-DA probe oxidation occurred after PDT exposure (i.e., the probe was added only after FICZ/UVA treatment), long-lived species (such as lipid- and protein-hydroperoxides) might be involved in the pro-oxidant chemistry downstream of photodynamic treatment causing probe oxidation, a possibility consistent with earlier considerations concerning the mechanistic limitations of DCF-DA as a probe of photooxidative stress, a topic discussed in much detail before (3, 4, 9, 28; and references therein). Likewise, we detected FICZ-PDT-induced loss of mitochondrial membrane potential (Fig. 5d), oxidative DNA damage (as assessed by Fpg-enhanced comet analysis; Fig. 5e), and lysosomal impairment (visualized by lysosensor staining; Fig. 5f). Strikingly, analogous stress response signaling (as detected before by immunoblot analysis in SCC-25 cells; Fig. 3e), characterized by rapid p38 MAPK and eIF2α phosphorylation, detectable together with upregulation of the common stress response proteins HSP70 and HO-1, occurred in A375 melanoma cells (Fig. 5g). Taken together, these data strongly suggest that the photodynamic activity of FICZ can be harnessed for the photooxidative elimination of cultured A375 malignant melanoma cells.

Photodynamic induction of cell death in reconstructed human epidermis and murine SKH-1 ‘high risk’ mouse skin exposed to the combined action of UVA and FICZ

After demonstrating FICZ-dependent UVA- and VIS-driven elimination of cultured malignant skin cancer cells (Figs. 2–5), we explored feasibility of achieving photodynamic induction of cell death in human reconstructed epidermis and mouse skin (Fig. 6). To this end, following our previously published research, we first employed human reconstructed epidermis incubated in growth medium supplemented with or without FICZ (100 nM; 6 h) followed by photon exposure (Fig. 6a). After FICZ treatment, specimens were exposed to UVA (6.6 J/cm^2) or VIS (LED 460 nm, 2.5 J/cm^2), and 24 h later specimens were analyzed for proteolytic cleavage of procaspase 3, a quantitative measure of cell death in response to photodynamic treatment. Indeed, basal keratinocytes stained positive for cleaved procaspase 3, an effect observed only in the most basal layer of those reconstructs (that had received

FICZ/UVA or FICZ/VIS combination treatment). Similar photodynamic effects were achieved in SKH-1 hairless mouse skin as a result of topical application of FICZ (dissolved in DMSO carrier) followed by UVA exposure, a treatment causing pronounced epidermal cellular damage as obvious from H&E staining and immunohistochemical detection of cleaved procaspase 3, effects observed throughout the entirety of the murine epidermis (Fig. 6b-c). Next, we pursued pilot experimentation testing feasibility of FICZ-dependent photodynamic intervention in 'high risk' tumor-prone mouse skin, a relevant *in vivo* model of UV-induced skin tumorigenesis (Fig. 6d). Specifically, after implementation of a chronic UVB exposure regimen over an eighteen week period, tumor-prone SKH1 'high risk' mice were subjected to three cycles of experimental FICZ-PDT [employing pre-application of topical FICZ (in DMSO as a carrier) followed by cutaneous UVA exposure]; tumor multiplicity was then determined at the end of the experiment (week twenty two). As a control, in parallel with high-risk mice receiving the complete FICZ-PDT regimen, mice were also undergoing 'UVA only', 'FICZ only', or mock treatment ('DMSO only'; no UVA). Indeed, in the FICZ-PDT group, the number of tumorous skin lesions per mouse (multiplicity) detectable at the end of the experiment was reduced by almost 35 % [(average multiplicity) control: 13.0; FICZ only: 12.8; UVA only: 11.3; FICZ/UVA: 8.7; $p < 0.05$], an effect consistent with FICZ-dependent photodynamic suppression of tumorigenic progression.

CONCLUSION

Endogenous photosensitizer chromophores may serve as promising pharmacophores for the development of PDT agents as substantiated by numerous historical examples (19). Taken together, our prototype data (generated in chemical model systems, cell culture, reconstructed human epidermis, and SKH1 mouse skin) demonstrate feasibility of harnessing the endogenous photosensitizer FICZ for the photodynamic elimination of malignant cells, achievable *in vitro* and *in vivo*. After observing that UVA-driven FICZ photosensitizer activity is associated with appreciable singlet oxygen quantum yield (Fig. 1), we assessed the photodynamic activity of FICZ against a panel of skin cancer cells, while substantiating the occurrence of extensive lysosomal, mitochondrial, and nuclear photooxidative damage associated with induction of caspase-independent cell death (Fig. 2–5). We also obtained prototype evidence that topical application of FICZ can cause the photodynamic suppression of UV-driven tumorigenesis in SKH1 hairless mouse skin (Fig. 6). Additional questions concerning specificity and preclinical efficacy of FICZ-dependent PDT targeting malignant skin cells remain to be answered. However, given (*i*) the endogenous nature of this tryptophan-derived photoproduct, (*ii*) its limited skin residence time due to rapid degradation through AhR-controlled CYP1A1-dependent catalysis, and (*iii*) its emerging physiological role in maintenance of skin barrier function, it is tempting to speculate that the pronounced phototoxic activity of FICZ may be harnessed for experimental and investigational photodynamic interventions targeting cutaneous malignancies in human skin.

ACKNOWLEDGEMENTS

Funding: Supported in part by grants from the National Institutes of Health [1R01CA229418 (PI: GW), 1R03CA230949 (PI: GW), 1R21ES029579 (PI: GW), 1P01CA229112, ES007091, ES006694, Arizona Cancer Center Support Grant CA023074]. The content is solely the responsibility of the authors and does not necessarily represent the official views of the National Cancer Institute or the National Institutes of Health.

REFERENCES

1. Sato K, Taguchi H, Maeda T, Minami H, Asada Y, Watanabe Y. and Yoshikawa K. (1995) The primary cytotoxicity in ultraviolet-a-irradiated riboflavin solution is derived from hydrogen peroxide, J Invest Dermatol, 105, 608–612. [PubMed: 7561167]
2. Menon EL and Morrison H. (2002) Formation of singlet oxygen by urocanic acid by UVA irradiation and some consequences thereof, Photochem Photobiol, 75, 565–569. [PubMed: 12081316]
3. Wondrak GT, Roberts MJ, Jacobson MK and Jacobson EL (2002) Photosensitized growth inhibition of cultured human skin cells: mechanism and suppression of oxidative stress from solar irradiation of glycated proteins, J Invest Dermatol, 119, 489–498. [PubMed: 12190875]
4. Wondrak GT, Roberts MJ, Jacobson MK and Jacobson EL (2004) 3-hydroxypyridine chromophores are endogenous sensitizers of photooxidative stress in human skin cells, J Biol Chem, 279, 30009–30020. [PubMed: 15133022]
5. Wondrak GT, Jacobson MK and Jacobson EL (2006) Endogenous UVA-photosensitizers: mediators of skin photodamage and novel targets for skin photoprotection, Photochem Photobiol Sci, 5, 215–237. [PubMed: 16465308]
6. Baier J, Maisch T, Maier M, Engel E, Landthaler M. and Baumler W. (2006) Singlet oxygen generation by UVA light exposure of endogenous photosensitizers, Biophys J, 91, 1452–1459. [PubMed: 16751234]
7. Ito K, Hiraku Y. and Kawanishi S. (2007) Photosensitized DNA damage induced by NADH: site specificity and mechanism, Free Radic Res, 41, 461–468. [PubMed: 17454128]
8. Serrano MP, Vignoni M, Lorente C, Vicendo P, Oliveros E. and Thomas AH (2016) Thymidine radical formation via one-electron transfer oxidation photoinduced by pterin: Mechanism and products characterization, Free Radic Biol Med, 96, 418–431. [PubMed: 27154982]
9. Justiniano R, Williams JD, Perer J, Hua A, Lesson J, Park SL and Wondrak GT (2017) The B6-vitamer Pyridoxal is a Sensitizer of UVA-induced Genotoxic Stress in Human Primary Keratinocytes and Reconstructed Epidermis, Photochem Photobiol, 93, 990–998. [PubMed: 28083878]
10. Tonolli PN, Chiarelli-Neto O, Santacruz-Perez C, Junqueira HC, Watanabe IS, Ravagnani FG, Martins WK and Baptista MS (2017) Lipofuscin Generated by UVA Turns Keratinocytes Photosensitive to Visible Light, J Invest Dermatol, 137, 2447–2450. [PubMed: 28711386]
11. Dougherty TJ, Grindey GB, Fiel R, Weishaupt KR and Boyle DG (1975) Photoradiation therapy. II. Cure of animal tumors with hematoporphyrin and light, J Natl Cancer Inst, 55, 115–121. [PubMed: 1159805]
12. Dougherty TJ (1984) Photodynamic therapy (PDT) of malignant tumors, Crit Rev Oncol Hematol, 2, 83–116. [PubMed: 6397270]
13. Dolmans DE, Fukumura D. and Jain RK (2003) Photodynamic therapy for cancer, Nat Rev Cancer, 3, 380–387. [PubMed: 12724736]
14. Robertson CA, Evans DH and Abrahamse H. (2009) Photodynamic therapy (PDT): a short review on cellular mechanisms and cancer research applications for PDT, J Photochem Photobiol B, 96, 1–8. [PubMed: 19406659]
15. Abrahamse H. and Hamblin MR (2016) New photosensitizers for photodynamic therapy, Biochem J, 473, 347–364. [PubMed: 26862179]
16. Khaydukov EV, Mironova KE, Semchishen VA, Generalova AN, Nechaev AV, Khochenkov DA, Stepanova EV, Lebedev OI, Zvyagin AV, Deyev SM and Panchenko VY (2016) Riboflavin

photoactivation by upconversion nanoparticles for cancer treatment, Sci Rep, 6, 35103. [PubMed: 27731350]

17. van Straten D, Mashayekhi V, de Bruijn HS, Oliveira S. and Robinson DJ (2017) Oncologic Photodynamic Therapy: Basic Principles, Current Clinical Status and Future Directions, Cancers (Basel), 9(2), pii: E19. [PubMed: 28218708]
18. Hamblin MR (2019) Photodynamic Therapy for Cancer: What's Past is Prologue, Photochem Photobiol, doi: 10.1111/php.13190; [Epub ahead of print].
19. Kessel D. (2019) Photodynamic Therapy: A Brief History, J Clin Med, 8(10), pii: E1581. [PubMed: 31581613]
20. Baptista MS, Cadet J, Di Mascio P, Ghogare AA, Greer A, Hamblin MR, Lorente C, Nunez SC, Ribeiro MS, Thomas AH, Vignoni M. and Yoshimura TM (2017) Type I and Type II Photosensitized Oxidation Reactions: Guidelines and Mechanistic Pathways, Photochem Photobiol, 93, 912–919. [PubMed: 28084040]
21. Fargnoli MC and Peris K. (2015) Photodynamic therapy for basal cell carcinoma, Future Oncol, 11, 2991–2996. [PubMed: 26550910]
22. Silva AP, Neves CL, Silva EDA, Portela TCL, Iunes RS, Cogliati B, Severino D, Baptista MDS, Dagli MLZ, Blazquez FJH and Silva J. (2018) Effects of methylene blue-mediated photodynamic therapy on a mouse model of squamous cell carcinoma and normal skin, Photodiagnosis Photodyn Ther, 23, 154–164. [PubMed: 29908976]
23. Hausmann W. (1911) The sensitising effect of haematoporphyrine., Biochem Z, 30, 276–316.
24. Meyer-Betz E. (1913) Untersuchungen ueber die biologische (photodynamische) Wirkung des Haematopophyrins und anderer Derivate des Blut- und Gallenfarbstoffes, Dtsch. Arch. Lin. Med, 112, 476–503.
25. Arboleda A, Miller D, Cabot F, Taneja M, Aguilar MC, Alawa K, Amescua G, Yoo SH and Parel JM (2014) Assessment of rose bengal versus riboflavin photodynamic therapy for inhibition of fungal keratitis isolates, Am J Ophthalmol, 158, 64–70 e62. [PubMed: 24792103]
26. Khan S, M.R. P, A Rizvi, M.M Alam, Rizvi Mand Naseem I. (2019) ROS mediated antibacterial activity of photoilluminated riboflavin: A photodynamic mechanism against nosocomial infections, Toxicol Rep, 6, 136–142. [PubMed: 30671349]
27. Rannug U, Rannug A, Sjoberg U, Li H, Westerholm R. and Bergman J. (1995) Structure elucidation of two tryptophan-derived, high affinity Ah receptor ligands, Chem Biol, 2, 841–845. [PubMed: 8807817]
28. Park SL, Justiniano R, Williams JD, Cabello CM, Qiao S. and Wondrak GT (2015) The Tryptophan-Derived Endogenous Aryl Hydrocarbon Receptor Ligand 6-Formylindolo[3,2-b]Carbazole Is a Nanomolar UVA Photosensitizer in Epidermal Keratinocytes, J Invest Dermatol, 135, 1649–1658. [PubMed: 25431849]
29. Justiniano R. and Wondrak GT (2016) The Aryl Hydrocarbon Receptor (AhR) as an Environmental Stress Sensor and Regulator of Skin Barrier Function, Skin Stress Response Pathways: Environmental Factors and Molecular Opportunities; Springer-Nature, 325–360.
30. Syed DN and Mukhtar H. (2015) FICZ: A Messenger of Light in Human Skin, J Invest Dermatol, 135, 1478–1481. [PubMed: 25964268]
31. Brem R, Macpherson P, Guven M. and Karran P. (2017) Oxidative stress induced by UVA photoactivation of the tryptophan UVB photoproduct 6-formylindolo[3,2-b]carbazole (FICZ) inhibits nucleotide excision repair in human cells, Sci Rep, 7, 4310. [PubMed: 28655934]
32. Vogeley C, Esser C, Tuting T, Krutmann J. and Haarmann-Stemmann T. (2019) Role of the Aryl Hydrocarbon Receptor in Environmentally Induced Skin Aging and Skin Carcinogenesis, Int J Mol Sci, 20(23), pii: E6005. [PubMed: 31795255]
33. Rannug A, Rannug U, Rosenkranz HS, Winqvist L, Westerholm R, Agurell E. and Grafstrom AK (1987) Certain photooxidized derivatives of tryptophan bind with very high affinity to the Ah receptor and are likely to be endogenous signal substances, J Biol Chem, 262, 15422–15427. [PubMed: 2824460]
34. Helferich WG and Denison MS (1991) Ultraviolet photoproducts of tryptophan can act as dioxin agonists, Mol Pharmacol, 40, 674–678. [PubMed: 1658604]

35. Fritsche E, Schafer C, Calles C, Bernsmann T, Bernshausen T, Wurm M, Hubenthal U, Cline JE, Hajimiragha H, Schroeder P, Klotz LO, Rannug A, Furst P, Hanenberg H, Abel J. and Krutmann J. (2007) Lightening up the UV response by identification of the arylhydrocarbon receptor as a cytoplasmatic target for ultraviolet B radiation, Proc Natl Acad Sci U S A, 104, 8851–8856. [PubMed: 17502624]

36. Smirnova A, Wincent E, Vikstrom Bergander L, Alsberg T, Bergman J, Rannug A. and Rannug U. (2016) Evidence for New Light-Independent Pathways for Generation of the Endogenous Aryl Hydrocarbon Receptor Agonist FICZ, Chem Res Toxicol, 29, 75–86. [PubMed: 26686552]

37. Rannug A. and Rannug U. (2018) The tryptophan derivative 6-formylindolo[3,2-b]carbazole, FICZ, a dynamic mediator of endogenous aryl hydrocarbon receptor signaling, balances cell growth and differentiation, Crit Rev Toxicol, 48, 555–574. [PubMed: 30226107]

38. Magiatis P, Pappas P, Gaitanis G, Mexia N, Melliou E, Galanou M, Vlachos C, Stathopoulou K, Skaltsounis AL, Marselos M, Velegraki A, Denison MS and Bassukas ID (2013) Malassezia yeasts produce a collection of exceptionally potent activators of the Ah (dioxin) receptor detected in diseased human skin, J Invest Dermatol, 133, 2023–2030. [PubMed: 23448877]

39. Wincent E, Bengtsson J, Mohammadi Bardbori A, Alsberg T, Luecke S, Rannug U. and Rannug A. (2012) Inhibition of cytochrome P4501-dependent clearance of the endogenous agonist FICZ as a mechanism for activation of the aryl hydrocarbon receptor, Proc Natl Acad Sci U S A, 109, 4479–4484. [PubMed: 22392998]

40. Youssef A, von Koschembahr A, Caillat S, Corre S, Galibert MD and Douki T. (2019) 6-Formylindolo[3,2-b]carbazole (FICZ) is a Very Minor Photoproduct of Tryptophan at Biologically Relevant Doses of UVB and Simulated Sunlight, Photochem Photobiol, 95, 237–243. [PubMed: 29882277]

41. Zhang C, Creech KL, Zuercher WJ and Willson TM (2019) Gram-scale synthesis of FICZ, a photoreactive endogenous ligand of the aryl hydrocarbon receptor, Sci Rep, 9, 9982. [PubMed: 31292477]

42. Tsuji G, Hashimoto-Hachiya A, Kiyomatsu-Oda M, Takemura M, Ohno F, Ito T, Morino-Koga S, Mitoma C, Nakahara T, Uchi H. and Furue M. (2017) Aryl hydrocarbon receptor activation restores filaggrin expression via OVOL1 in atopic dermatitis, Cell Death Dis, 8, e2931. [PubMed: 28703805]

43. Kiyomatsu-Oda M, Uchi H, Morino-Koga S. and Furue M. (2018) Protective role of 6-formylindolo[3,2-b]carbazole (FICZ), an endogenous ligand for arylhydrocarbon receptor, in chronic mite-induced dermatitis, J Dermatol Sci, 90, 284–294. [PubMed: 29500077]

44. Justiniano R, Perer J, Hua A, Fazel M, Krajisnik A, Cabello CM and Wondrak GT (2017) A Topical Zinc Ionophore Blocks Tumorigenic Progression in UV-exposed SKH-1 High-risk Mouse Skin, Photochem Photobiol, 93, 1472–1482. [PubMed: 28503778]

45. Uchoa AF, Knox PP, Turchielle R, Seifullina N. and Baptista MS (2008) Singlet oxygen generation in the reaction centers of Rhodobacter sphaeroides, Eur Biophys J, 37, 843–850. [PubMed: 18286272]

46. Tasso TT, Schlothauer JC, Junqueira HC, Matias TA, Araki K, Liandra-Salvador E, Antonio FCT, Homem-de-Mello P. and Baptista MS (2019) Photobleaching Efficiency Parallels the Enhancement of Membrane Damage for Porphyrazine Photosensitizers, J Am Chem Soc, 141, 15547–15556. [PubMed: 31490678]

47. Meade-Tollin LC, Boukamp P, Fusenig NE, Bowen CP, Tsang TC and Bowden GT (1998) Differential expression of matrix metalloproteinases in activated c-ras-Ha-transfected immortalized human keratinocytes, Br J Cancer, 77, 724–730. [PubMed: 9514050]

48. Williams JD, Bermudez Y, Park SL, Stratton SP, Uchida K, Hurst CA and Wondrak GT (2014) Malondialdehyde-derived epitopes in human skin result from acute exposure to solar UV and occur in nonmelanoma skin cancer tissue, J Photochem Photobiol B, 132, 56–65. [PubMed: 24584085]

49. Lamore SD and Wondrak GT (2013) UVA causes dual inactivation of cathepsin B and L underlying lysosomal dysfunction in human dermal fibroblasts, J Photochem Photobiol B, 123, 1–12. [PubMed: 23603447]

50. Davis AL, Qiao S, Lesson JL, Rojo M. de la Vega, Park SL, Seanez CM, Gokhale V, Cabello CM and Wondrak GT (2015) The quinone methide aurin is a heat shock response inducer that causes

proteotoxic stress and Noxa-dependent apoptosis in malignant melanoma cells, J Biol Chem, 290, 1623–1638. [PubMed: 25477506]

51. Hua AB, Justiniano R, Perer J, Park SL, Li H, Cabello CM and Wondrak GT (2019) Repurposing the Electron Transfer Reactant Phenazine Methosulfate (PMS) for the Apoptotic Elimination of Malignant Melanoma Cells through Induction of Lethal Oxidative and Mitochondriotoxic Stress, Cancers (Basel), 11 (5), pii:E1369. [PubMed: 31540086]
52. Kessel D. and Reiners JJ Jr. (2015) Promotion of Proapoptotic Signals by Lysosomal Photodamage, Photochem Photobiol, 91, 931–936. [PubMed: 25873082]
53. Tsubone TM, Martins WK, Pavani C, Junqueira HC, Itri R. and Baptista MS (2017) Enhanced efficiency of cell death by lysosome-specific photodamage, Sci Rep, 7, 6734. [PubMed: 28751688]

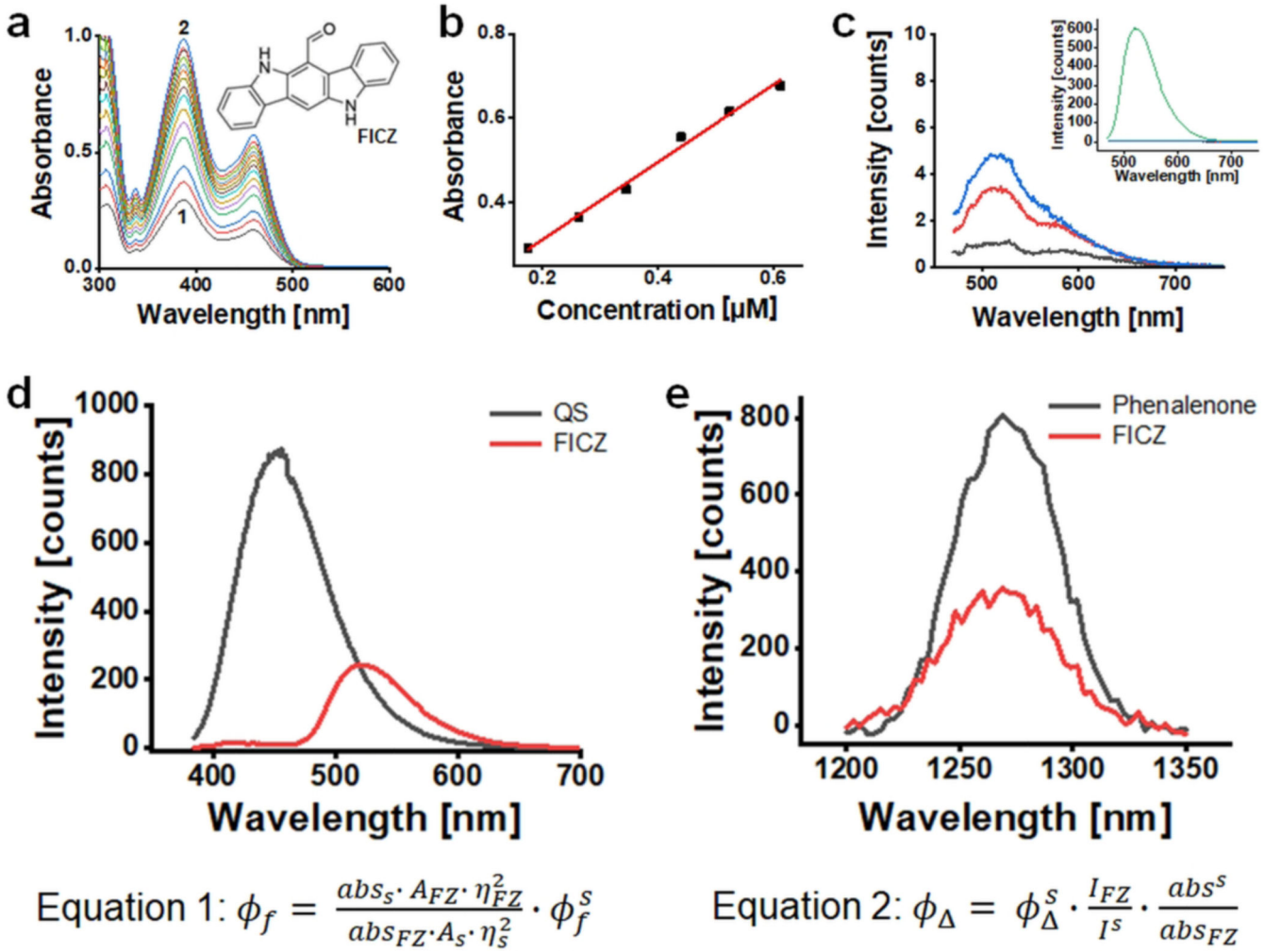

Figure 1. Photophysical properties of FICZ.

(a) Absorbance spectra of FICZ in methanol at different concentrations from 1 to 2, FICZ concentration changed from 17.6 μM to 138.6 μM. Insert depicts FICZ chemical structure. (b) Molar extinction coefficients at 390 nm, ε = 9180 $Lmol^{-1}cm^{-1}$. (c) Fluorescence spectra of FICZ in methanol and in aqueous BSA solutions; insert: FICZ emission spectra in methanol (green) and in aqueous solutions (baseline); main panel: amplification of FICZ emission spectra in aqueous solutions at different BSA concentrations varying from pure water (black) to [BSA]= 15 μM (red) and 30 μM (blue) [FICZ]=17 μM; (d) Fluorescence spectra of quinine sulfate (QS) in 0.5 $molL^{-1}$ sulfuric acid solution (black) and of FICZ in methanol (red), [FICZ]=7.7 μM; [QS]=12.4 μM; λ_{ex} = 355 nm, Abs_{355nm}=0.07, slits=10 mm. *Equation 1* was used to calculate the fluorescence quantum yield (Φ_f), where abs, A and n are respectively absorbance at 355, integrated area under the spectra and solvent refractive index, s and FZ are standard and FICZ, respectively. (e) Singlet oxygen emission spectra in methanol solutions of phenalenone (black) and of FICZ (red). [FICZ]=27 μM; [phenalenone]=23 μM λ_{ex} = 355 nm, Abs_{355nm}=0.2. *Equation 2* was used to calculate the quantum yield of singlet oxygen generation (Φ_Δ), where I is integrated emission, abs is absorbance at the excitation wavelength, s and FZ are standard and FICZ, respectively.

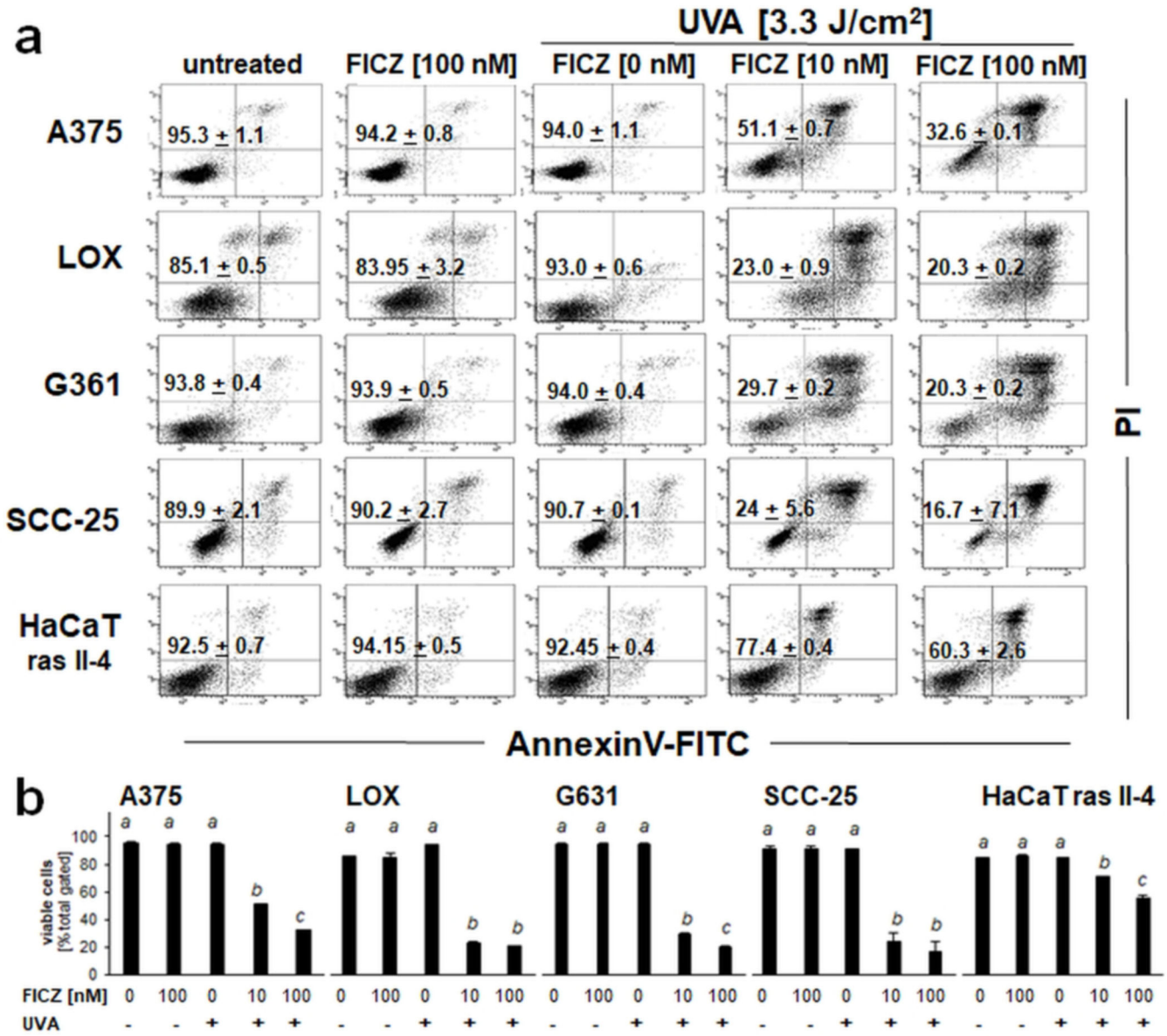

Figure 2. Photodynamic elimination of cultured human skin cancer cells exposed to the combined action of UVA and FICZ.

A panel of cultured human malignant skin cell lines (A375 melanoma, LOX melanoma, G361 melanoma, SCC-25, HaCaT-ras II-4 keratinocytes) was exposed to the isolated or combined action of FICZ (10–100 nM) and UVA (3.3 J/ cm^2). Control cells remained untreated. After 24 h, cell viability was determined by flow cytometric analysis of annexinV (AV)-FITC/propidium iodide (PI)-stained cells. (a) Numbers indicate viable cells (AV^-/PI^-) as a percentage of total gated cells [n =3; mean ± SEM]. (b) Bar graph depiction of quantitative data analysis (per cell type) employing ANOVA with Tukey's post hoc test; means without a common letter differ from each other ($p<0.05$).

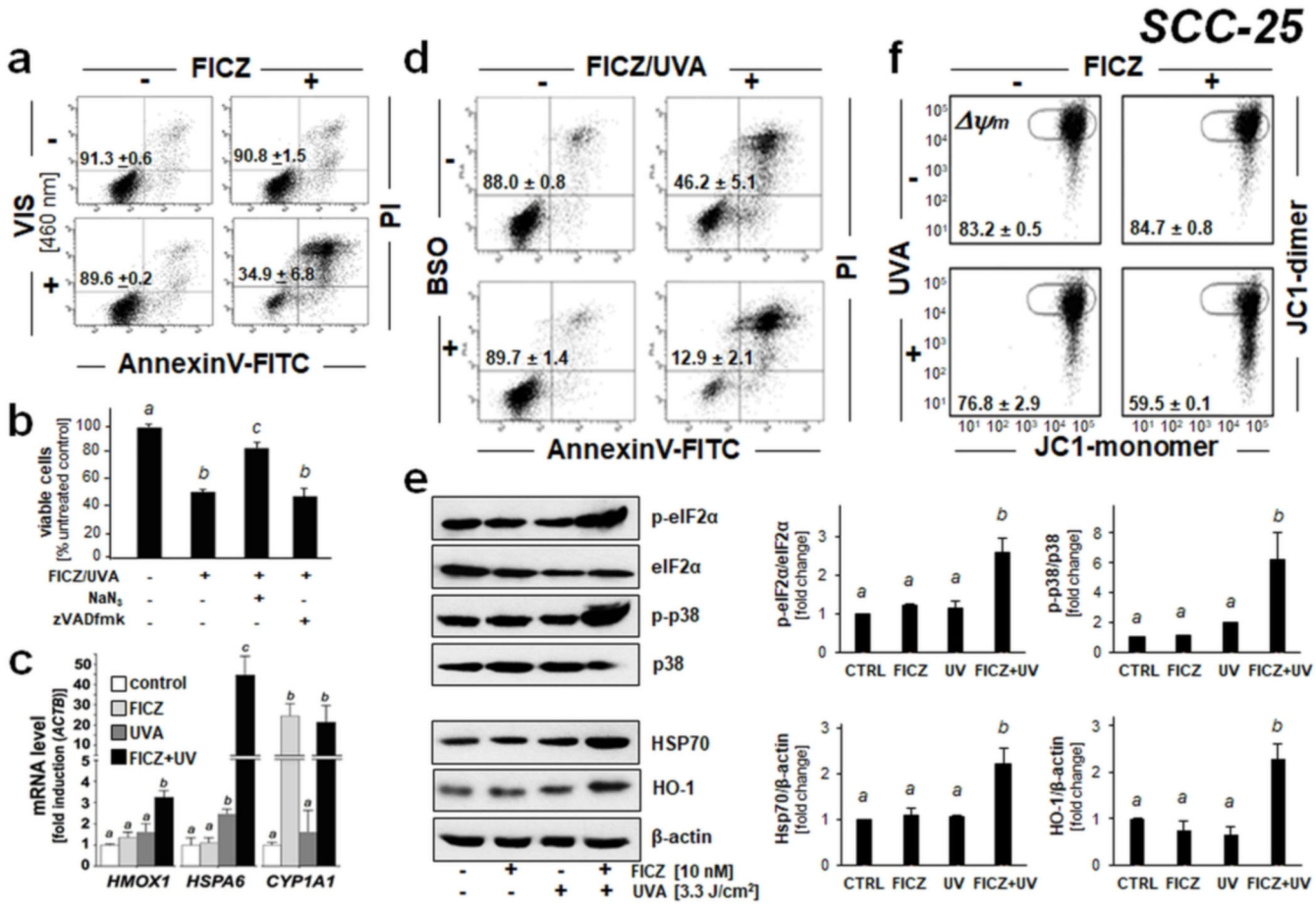

Figure 3. FICZ-dependent photodynamic induction of stress response gene expression and signaling in SCC-25 keratinocytes.

(a) Cells were exposed to the combined or isolated action of FICZ (10 nM) and blue light [LED 460 nm; 2.5 J/cm^2]. After 24 h, cell viability was determined by flow cytometry as described in Fig. 2 [mean ± SD, n = 3]. (b) Cells were exposed to FICZ-PDT [FICZ: 100 nM; UVA: 3.3 J/cm^2] with or without the inclusion of NaN_3 (10 mM) or zVADfmk (40 μM; 1 h before and until 24 h after PDT). After 24 h, viability was determined as in Fig. 2. (c) Stress response gene expression 6 h after FICZ-UVA [FICZ 10 nM; UVA 3.3 J/cm^2] treatment was determined at the mRNA level [fold induction versus *ACTB*; n =3; mean + SD]. (d) Effects of FICZ/UVA on cell viability were examined after pharmacological glutathione depletion [buthionine sulfoximine (BSO): 1 mM, 24 h pretreatment; conditions as in Fig. 2]. (e) Cellular stress response induced by FICZ-UVA [FICZ 10 nM; UVA 3.3 J/cm^2; top panel: 1h after irradiation; bottom panel: 6 h after irradiation] as determined at the protein level (immunoblot analysis; n≥3); bar graphs depict quantitative analysis (versus loading control as indicated). (f) Loss of mitochondrial transmembrane potential (Δψm) was assessed by flow cytometric analysis of JC-1 stained cells, 1 h after FICZ [FICZ: 10 nM; UVA: 3.3 J/cm^2] treatment. Numbers indicate percentage of cells inside the circle displaying intact Δψm [n=3, mean ± SD; ($p<0.05$)]. For all bar graph depictions, quantitative data analysis employed ANOVA with Tukey's post hoc test; means without a common letter differ from each other ($p<0.05$).

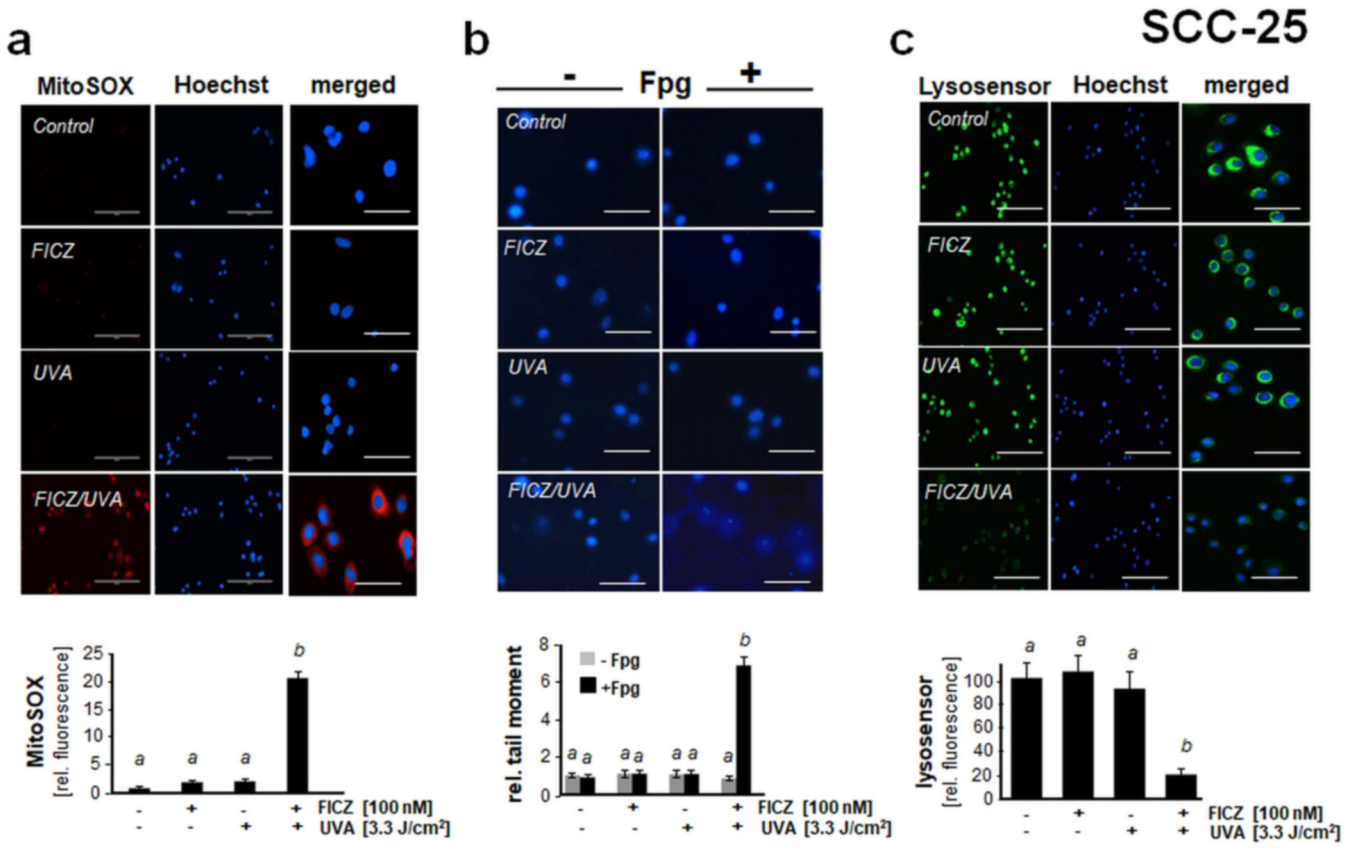

Figure 4. Photodynamic impairment of mitochondrial, lysosomal, and nuclear genomic integrity in SCC-25 keratinocytes exposed to the combined action of UVA and FICZ.

(a) Mitochondrial superoxide generation by FICZ-PDT [FICZ 100 nM; UVA 3.3 J/cm^2; 1 h] was detected using MitoSOX Red™ fluorescence microscopy. Bar graph displays quantitative analysis of relative fluorescence intensity [n=85, mean ± SEM; scale bar: 200 μm (left and middle panels); 40 μm (overlay)]. (b) Genomic integrity was assessed using the Fpg-enhanced comet assay [FICZ: 100 nM; UVA: 3.3 J/cm^2; 1 h]. Bar graph displays quantitative analysis of relative comet moment [n=50 per group, mean ± SEM]. (c) FICZ-PDT-induced lysosomal impairment [FICZ 100 nM; UVA 3.3 J/cm^2; 1 h] as analyzed using LysoSensor green fluorescence microscopy [scale bar: 200 μm, 40 μm (overlay); n=85, mean ± SEM]. Bar graph displays quantitative analysis of LysoSensor fluorescence intensity [n=85, mean ± SEM]. For bar graph depiction, quantitative data analysis employed ANOVA with Tukey's post hoc test; means without a common letter differ from each other (p<0.05).

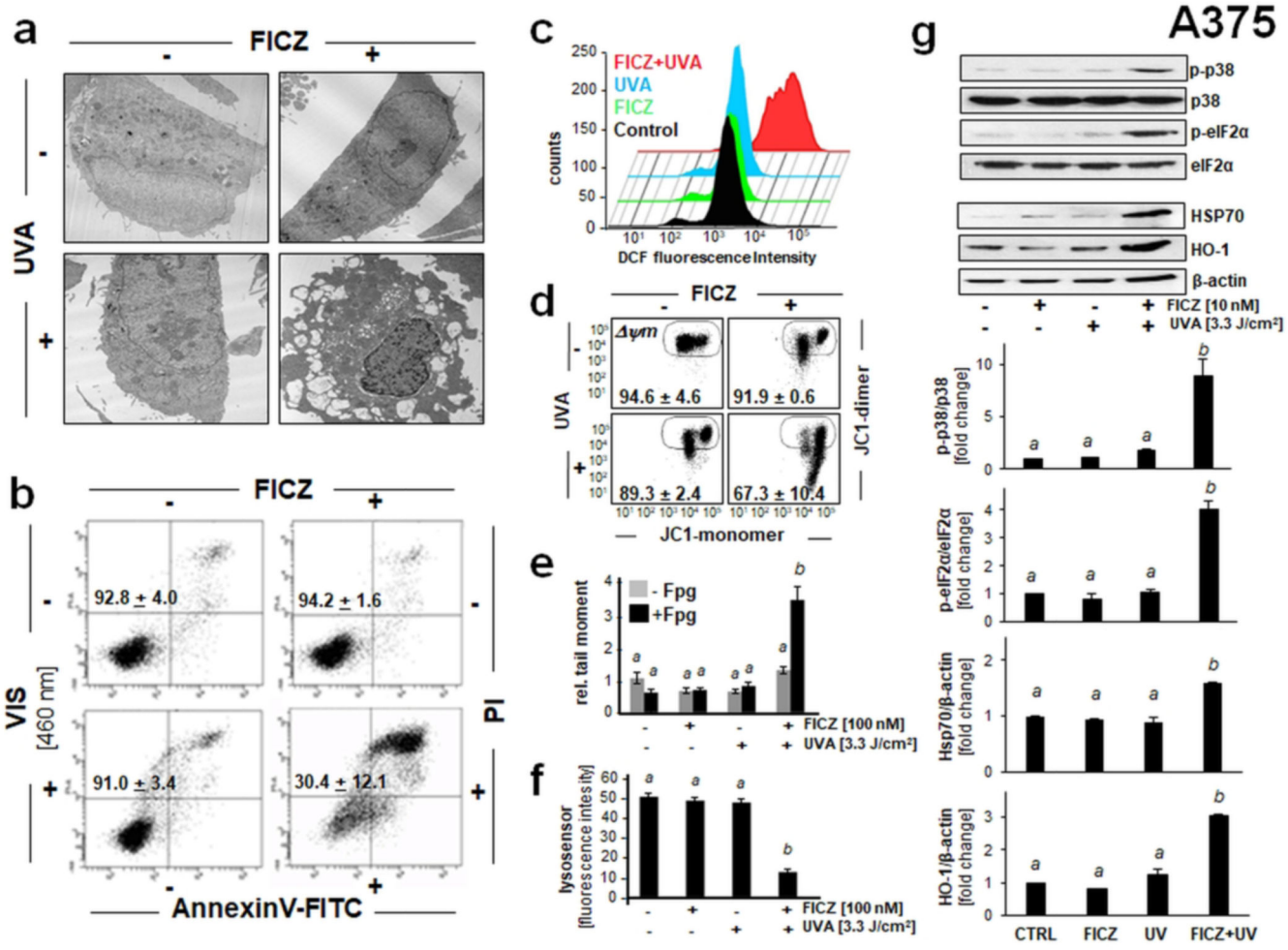

Figure 5. Photodynamic induction of stress response gene expression in A375 malignant melanoma cells exposed to the combined action of UVA and FICZ.

(a) Transmission electron microscopy (fold magnification: x 2,650) 6 h after FICZ-PDT (FICZ 100 nM; UVA 3.3 J/cm^2). (b) Cells exposed to FICZ [10 nM] and blue light [LED 460 nm, 2.5 J/cm^2]. Flow cytometric analysis of annexinV-FITC/propidium iodide (PI)-stained cells [24 h; n=3, mean ± SEM]. (c) Induction of cellular oxidative stress as examined 1 h after FICZ-PDT (conditions as in A) using flow cytometric analysis of DCF-DA stained cells. A representative experiment (out of at least three representative repeats) is displayed. (d) Loss of mitochondrial transmembrane potential (Δψm) as assessed by flow cytometric analysis of JC-1 stained cells, 1 h after FICZ (10 nM)/UVA (3.3 J/cm^2) treatment. Numbers indicate percentage of cells inside the circle displaying intact Δψm [n=3, mean ± SD; ($p<0.05$)]. (e) Fpg-enhanced comet assay [FICZ: 100 nM; UVA: 3.3 J /cm^2; 1 h] as performed in Fig. 4b. Bar graph displays relative comet tail moment [n=50 per group; mean ± SEM]. (f) FICZ-PDT-induced lysosomal impairment [FICZ 100 nM; UVA 3.3 J/cm^2; 1 h] detected by LysoSensor green fluorescence microscopy [scale bar: 200 μm, 40 μm (overlay); n=85, mean ± SEM]. Bar graph displays quantitative analysis of LysoSensor fluorescence intensity [n=85, mean ± SEM]. (g) Cellular stress response induced by FICZ-UVA [FICZ 10 nM; UVA 3.3 J/cm^2; top panel: 1h after irradiation; bottom panel: 6 h after irradiation] as

determined at the protein level (immunoblot analysis; n≥3). For bar graph depiction, quantitative data analysis employed ANOVA with Tukey's post hoc test; means without a common letter differ from each other ($p<0.05$).

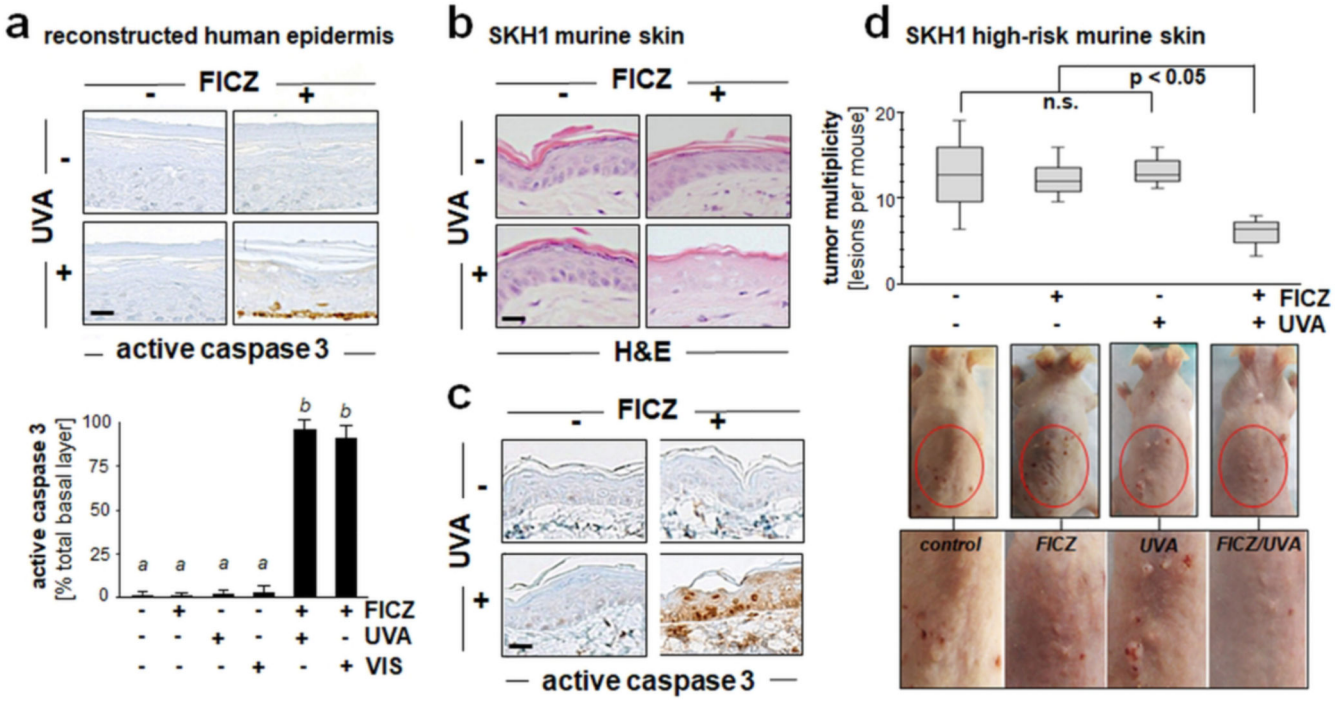

Figure 6. Photodynamic induction of cell death in reconstructed human epidermis and murine SKH-1 'high risk' mouse skin exposed to the combined action of UVA and FICZ.

(a) Epidermal reconstruct (Epiderm™) specimens were cultured in growth medium supplemented with or without FICZ (100 nM; 6 h). After culture, reconstructs were placed in PBS followed by UVA [6.6 J/cm^2; panel (a)] or VIS exposure (LED 460 nm, 2.5 J/cm^2; images not shown). After 24 h, percentage apoptotic keratinocytes staining positive for cleaved procaspase 3 versus total basal keratinocytes was determined (n=3, mean ± SD)]. For bar graph depiction, quantitative data analysis employed ANOVA with Tukey's post hoc test; means without a common letter differ from each other (p<0.05). (b-c) SKH-1 hairless mice (n=3 per treatment group) were exposed to the isolated or combined action of topical FICZ (1 mM in DMSO) and UVA (6.6 J/cm^2) radiation. 48 h after treatment, H&E (panel b) and IHC [cleaved (active) procaspase 3; panel c] analysis revealed photodynamic effects including epidermal necrosis. Per treatment group, representative images taken from three repeat samples are displayed (scale bars = 25 μm). (d) After being subjected to a chronic UVB exposure regimen [≤ 190 mJ/cm^2; three times per week; 18 weeks], tumor-prone SKH-1 'high risk' mice were undergoing experimental FICZ-PDT [topical application; 10 mM in DMSO; 6.6 J/cm^2 UVA; 3 PDT treatment cycles]. Additional mice were exposed to 'UVA only', 'FICZ only', or 'mock' (DMSO) treatment (n = 4 mice per group) followed by examination of tumor multiplicity (number of lesions per mouse) at the end of the treatment regimen (week 22). Box plot indicates interquartile range and average tumor multiplicity (non-parametric Mann-Whitney test; $p < 0.05$). Representative images are displayed with red circles marking back skin area undergoing FICZ-PDT at the end of the experiment (enlarged in the bottom panel).